Jurnal Kejuruteraan 36(4) 2024: 1409–1422
https://doi.org/10.17576/jkukm-2024-36(4)-07

Performance Comparison and Analysis of Four- and Six-Switch Inverter Controls of BLDC Motor Employing Deep Learning

Musa Mohammed Gujja, Dahaman Ishak*, Muhammad Najwan Hamidi & Mohamed Salem

School of Electrical and Electronic Engineering, Universiti Sains Malaysia, Nibong Tebal, Penang, Malaysia,

**Corresponding author: dahaman@usm.my*

Received 16 January 2024, Received in revised form 12 March 2024
Accepted 12 April 2024, Available online 30 July 2024

ABSTRACT

Robust and effective control of brushless dc (BLDC) motors is paramount in modern-day motion control. The BLDC motor is known for its high speed, high torque, small size, low noise, and equally low maintenance requirements compared to the brushed DC motor. Nowadays, it can be found in the areas of robotics, aerospace, military, and industrial machines, among others. In this paper, two inverter topologies, the three-phase six-switch driver circuit (TPSSDC) and the three-phase four-switch driver circuit (TPFSDC), are used to drive and control the speed of the BLDC motor. For the control technique, however, a fitting neural network from the deep learning (DL) toolbox is employed to train and improve the speed performance of the motor. Both TPSSDC and TPFSDC are simulated and tested in MATLAB Simulink, and the resultant output is analyzed graphically and analytically. Graphical observation shows that the TPSSDC control approach is superior in terms of reference tracking and has less ripple, and better rise and settling times when compared to the TPFSDC control approach, however, the TPFDC is considered for its low cost and simple circuitry. Numerically, the TPSSDC also outperforms at 1000 rpm with a 1.685 ms rise time and a 1.420 ms settling time compared to the TPFSDC, which rises at 6.526 ms and settles at 5.237 ms. At 3000 rpm motor speed, the TPSSDC is better, having a rise time of 5.815 ms and settling time of 4.048 ms, when compared to the TPFSDC, which rises at 11.277 ms and settles at 10.067 ms.

Keywords: BLDC motor; speed control; inverter topology; deep learning; neural networks

INTRODUCTION

The importance of electrical equipment and motion control in modern times cannot be over-emphasized due to their wide range of applications. Therefore, enhancements for more effective motion control are on the rise. The drive and control of the BLDC motor are intuitively challenging, as new control strategies always emerge. Many researchers have worked on motion control using different techniques to achieve high speed and efficiency. Mostly, the six- and four-switch driving techniques are considered. The six-switching driving topology is the conventional method with six switches. Ale (2022), conducted a study on analysing the performance of an in-wheel BLDC motor employing a six-switching strategy, the PID controller is used to regulate the speed of the motor. de Almeida et al. (2020) also used six-switching to drive the motor with a variable speed robust control, this was achieved by employing a convex optimization approach. More so, additional control approaches might be incorporated to control and optimize the performance of a motor which works with either six or four switching inverters such as Surabhi et al. (2017) who worked on six switching inverters using a particle swarm optimization method in conjunction with fuzzy logic controller to boost the performance of the motor. The resultant output of the technique is compared with that of the PID controller for optimum results. Equally, Vikhe et al. (2019) and Wang et al. (2020) worked on six switching inverter topologies and a neural network was utilized to control the speed of a motor. The resultant output of the neural network is analysed mathematically and compared equally for good workability. The Artificial Intelligence control technique is a data-driven method, with branches such as machine learning and deep learning

which have recently been used to train and optimize the motor's performance (L. Saleh et al. 2021; Lajić & Matić 2022; Yao et al. 2023). Consequently, it has been proven by several works that the artificial neural network can be used to attain optimum speed control (Al Mashhadany et al. 2022; Pamuji et al. 2022; Saleh et al. 2022). Likewise, more controllers can be incorporated together, such as the model reference adaptive control and the artificial neural network, to resolve a nonlinearity problem as discussed by Archana and Dr Unde (2019). The technique attained a tremendous improvement in system efficiency. While Didi et al, (2017) and Huang et al, (2020) utilized the model reference adaptive control to achieve optimum speed. Also, modern work shows that comparing the performance of the motor using different inverter topologies in view to determine the best control approach for an efficient motor drive is crucial here, Gujja and Ishak (2023) illustrated and matched the system performance based on six and four switching inverters to ascertain the best driving topology, PID parameters are tuned using optimization techniques to attain optimum performance. In the case of Özge Gülbaş et al. (2020), the PI-based particle swarm and sine-cosine optimization approach was applied to improve the system efficiency and to minimize overshot, a decay coefficient is used in the fitness function. Additionally, experiments were carried out by some researchers to validate their simulation findings (Arun Prasad & Nair, 2020; Vanchinathan et al. 2021). Moreover, consideration has been given lately to a cost-effective four-switching driving topology for its low-cost and less complex structure. Naseri et al. (2021) and Safak et al. (2016) show the BLDC motors control employing the four-switching driving method is achievable and the performance is similar to the six-switching inverter topology. However, both topologies can be implemented using both open and closed-loop control techniques, the closed is preferred for its accuracy due to the feedback system (Mohd Zaihidee et al. 2022; Reddy et al. 2023).

Considering some of the problems from previous work such as overshoot, undershoot, low rise and settling time during operation which led to low performance. To curtail the problem the fitting neural network from the deep learning toolbox was employed for its ability to effectively train and precisely imitate the motor's behaviour for previously untrained data minimizing the overshoot and undershot as well as improving the system rise and settling time ensuring the output speed agrees with the reference speed.

Therefore, this paper intends to comprehensively compare the performance of the motor using both the TPSSDC and TPFSDC topology. The performance is analysed both graphically and numerically which aims to precisely ascertain the best control and driving strategy for the BLDC motor. Also, a neural network from the deep learning control toolbox is used to train and predict the future system response for effective speed control. This is possible by collecting the data of the reference input and the resultant speed output of the model. These collected data are employed by the neural networks to train the model and predict the best future response. Figure 1 (a) and (b) show typical topologies of TPSSDC and TPFSDC respectively. TPSSDC is a conventional six-switch inverter, while TPFSDC has only four switches and two capacitors. The two capacitors can be connected in series in any phase leg. Therefore, the controller has only four switches to regulate the motor's phase windings, hence, the motor speed and torque.

The article's structure encompasses the methodology of the proposed technique which vividly discusses the motor modelling, TPSSDC and TPFSDC control strategy and deep learning neural network control approach. The result and discussion section shows the resultant waveform and analyses of the numerical values while the conclusion section summarizes the article's findings.

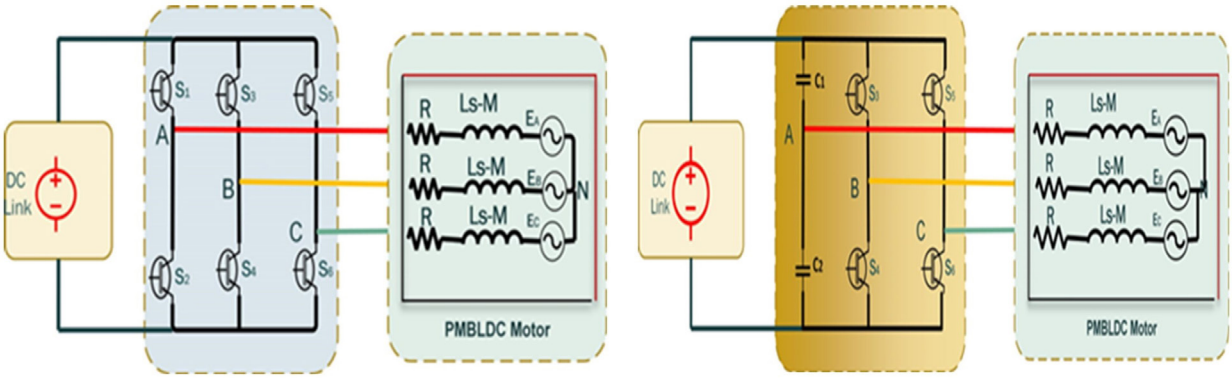

FIGURE 1. (a) TPSSDC topology, (b) TPFSDC topology

METHODOLOGY

MODELLING OF A BLDC MOTOR

The three-phase BLDC motor can be described in an analytical model, with few assumptions such as ignoring the saturation effect of the iron cores and uniform airgap in the machine. The hall-effect sensors are placed at 120^0 electrical symmetrically in order to predict the exact rotor position for the correct phase commutation sequence.

TPSSDC FOR BLDC MOTOR CONTROL

The TPSSDC arrangement is the usual driving approach. In this work, the IGBT was utilized for its high power and fast switching abilities; six IGBTs were also used as switches i.e. S_1, S_2, S_3, S_4, S_5, and S_6 respectively. In this technique, only two phases will be active at a time. Moreover, a controller can be incorporated to boost the system's performance. Figure 2 shows the complete system model. While Figure 3 illustrates the TPSSDC switching sequence and Table 1 shows the switching patterns. The voltage equations of TPSSDC can be represented as given below. Considering the three-phase neutral point N of Y-connected windings.

$$\begin{bmatrix} V_{AN} \\ V_{BN} \\ V_{CN} \end{bmatrix} = \begin{bmatrix} R_s & 0 & 0 \\ 0 & R_s & 0 \\ 0 & 0 & R_s \end{bmatrix} \begin{bmatrix} i_A \\ i_B \\ i_C \end{bmatrix} + \frac{d}{dt} \begin{bmatrix} L-M & 0 & 0 \\ 0 & L-M & 0 \\ 0 & 0 & L-M \end{bmatrix} \begin{bmatrix} i_A \\ i_B \\ i_C \end{bmatrix} + \begin{bmatrix} E_A \\ E_B \\ E_C \end{bmatrix} \quad (1)$$

where: V_{AN}, V_{BN}, and V_{CN} are the phase voltages, M is the mutual inductance, and L represents the self-inductance, $i_A, i_B, and\ i_C$ are the phases currents, E_A, E_B, and E_C are the phase back-emfs. For symmetrical phase windings, the phase resistances are equal and denoted as R_S.

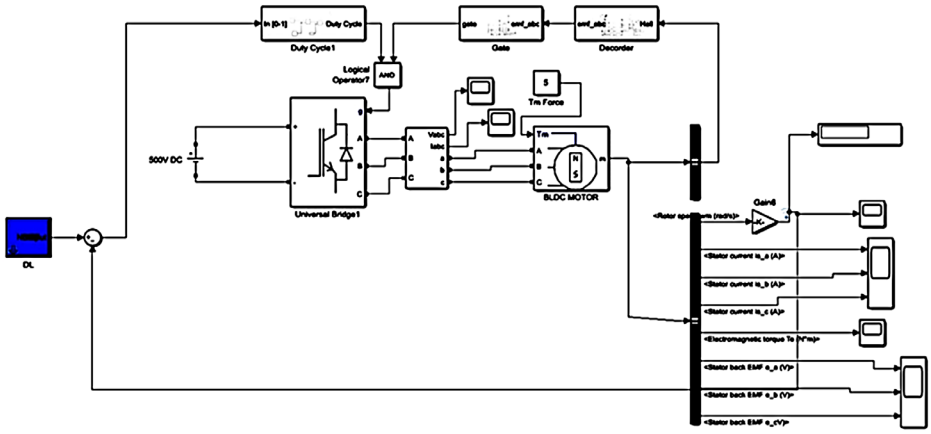

FIGURE 2. Complete model of TPSSDC with BLDC motor in MATLAB Simulink

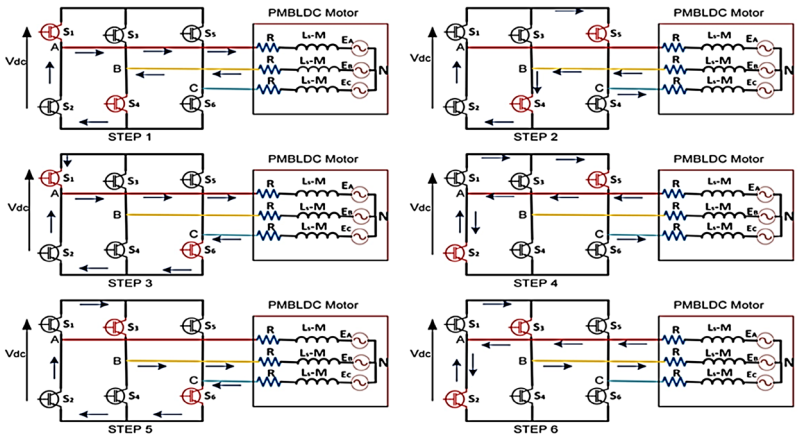

FIGURE 3. TPSSDC switching patterns

TABLE 1. Six-step switching sequence for TPSSDC

Steps	Switches	Active Phases	Silent Phase
1	S_1, S_4	A, B	C
2	S_5, S_4	C, B	A
3	S_1, S_6	A, C	B
4	S_5, S_2	C, A	B
5	S_3, S_6	B, C	A
6	S_3, S_2	B, A	C

TPFSDC FOR BLDC MOTOR CONTROL

This inverter uses only four IGBTs. The switches are S_1, S_2, S_3, and S_4, while capacitors C_1 and C_2 are connected in series, and their midpoint is connected to the terminal phase A winding of the BLDC motor. In this topology, being connected to the capacitors, the motor's phase A winding cannot be controlled. An appropriate motor controller should be incorporated with the inverter for effective speed control. Considering the voltage from motor terminals to the neutral point N, the TPFSDC voltage equations can be represented by.

$$V_{AN} = R_s i_A + L\frac{di_A}{dt} + M\left[\frac{di_B}{dt} + \frac{di_C}{dt}\right] + E_A \quad (2)$$

$$V_{BN} = R_s i_B + L\frac{di_B}{dt} + M\left[\frac{di_A}{dt} + \frac{di_C}{dt}\right] + E_B \quad (3)$$

$$V_{CN} = R_s i_C + L\frac{di_C}{dt} + M\left[\frac{di_A}{dt} + \frac{di_B}{dt}\right] + E_C \quad (4)$$

So, the equations (2) to (4) can be arranged in a Matrix state-space form as:

$$\begin{bmatrix} V_{AN} \\ V_{BN} \\ V_{CN} \end{bmatrix} = \begin{bmatrix} R_s & 0 & 0 \\ 0 & R_s & 0 \\ 0 & 0 & R_s \end{bmatrix} \begin{bmatrix} i_A \\ i_B \\ i_C \end{bmatrix} + \frac{\mathrm{d}}{dt} \begin{bmatrix} L_{AA} & L_{AB} & L_{AC} \\ L_{BC} & L_{BB} & L_{BC} \\ L_{CA} & L_{CB} & L_{CC} \end{bmatrix} \begin{bmatrix} i_A \\ i_B \\ i_C \end{bmatrix} + \begin{bmatrix} E_A \\ E_B \\ E_C \end{bmatrix} \quad (5)$$

Let the magnetic coupling between phases be:

$$L_{AB} = L_{AC} = L_{BA} = L_{BC} = L_{CA} = L_{CB} = M \quad (6)$$

where: M is the mutual inductance and L stands for the self-inductance. Substituting (6) in (5), it yields.

$$\begin{bmatrix} V_{AN} \\ V_{BN} \\ V_{CN} \end{bmatrix} = \begin{bmatrix} R_s & 0 & 0 \\ 0 & R_s & 0 \\ 0 & 0 & R_s \end{bmatrix} \begin{bmatrix} i_A \\ i_B \\ i_C \end{bmatrix} + \frac{\mathrm{d}}{\mathrm{dt}} \begin{bmatrix} L & M & M \\ M & L & M \\ M & M & L \end{bmatrix} \begin{bmatrix} i_A \\ i_B \\ i_C \end{bmatrix} + \begin{bmatrix} E_A \\ E_B \\ E_C \end{bmatrix} \quad (7)$$

Let the three-phase current equation be:

$$i_A + i_B + i_C = 0 \quad (8)$$

The inductance matrix in the system can be written as:

$$Mi_B + Mi_C = -Mi_A \quad (9)$$

Similarly,

$$V_{AN} = R_s i_A + (L - M)\frac{di_A}{dt} + E_A \quad (10)$$

$$V_{BN} = R_s i_B + (L - M)\frac{di_B}{dt} + E_B \quad (11)$$

$$V_{CN} = R_s i_C + (L - M)\frac{di_C}{dt} + E_C \quad (12)$$

Recall that the voltage obtained from point A to N with TPFSDC is represented as:

$$V_{AN} = R_s i_A + (L - M)\frac{di_A}{dt} + e_A + V_{c1} \quad (13)$$

Where: C is equal to C_1 and C_2, and voltages across them are V_{c1} and V_{c2} respectively, the input voltage is represented as V_{DC}. Thus, the voltage in the capacitor can be assumed as the DC voltage and voltage variation.

$$V_{c1} = \frac{V_{DC}}{2} - V_c \quad (14)$$

Likewise

$$V_{c2} = \frac{V_{DC}}{2} - V_c \tag{15}$$

Consequently, the voltage variation can be deduced as

$$V_c = \frac{-1}{2C} \int i_c(t)dt \tag{16}$$

The voltage amplitude variation is directly linked to the amplitude of phase current i_A, speed and the value of the capacitor.

Therefore, the equation can further be deduced as

$$\begin{bmatrix} V_{AN} \\ V_{BN} \\ V_{CN} \end{bmatrix} = \begin{bmatrix} R_s & 0 & 0 \\ 0 & R_s & 0 \\ 0 & 0 & R_s \end{bmatrix} \begin{bmatrix} i_A \\ i_B \\ i_C \end{bmatrix} + \frac{\mathrm{d}}{\mathrm{dt}} \begin{bmatrix} L-M & 0 & 0 \\ 0 & L-M & 0 \\ 0 & 0 & L-M \end{bmatrix} \begin{bmatrix} i_A \\ i_B \\ i_C \end{bmatrix} + \begin{bmatrix} E_A \\ E_B \\ E_C + V_{c1} \end{bmatrix} \tag{17}$$

Figure 4 is the TPFSDC complete model. Whereas, Figure 5 shows the switching patterns, and Table 2 indicates the TPFSDC switching sequence.

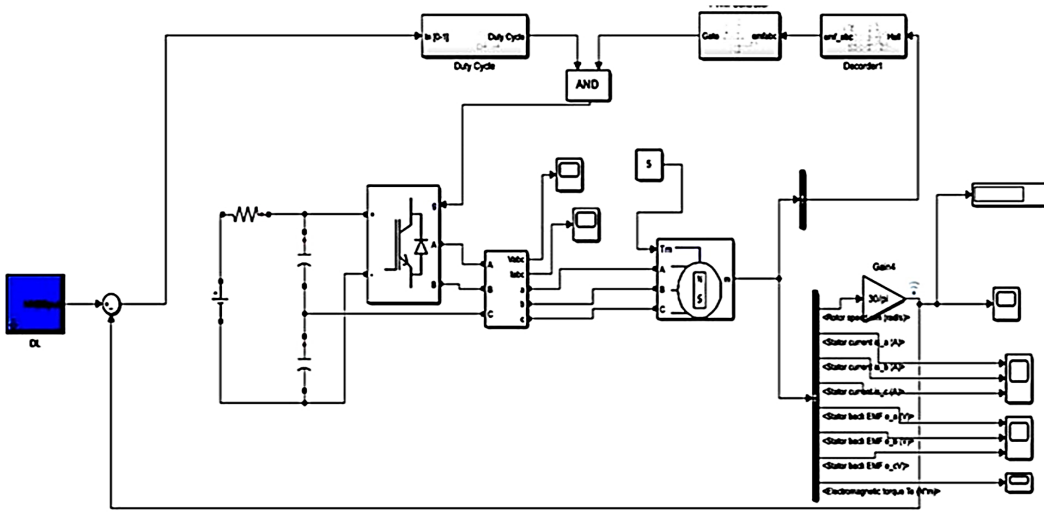

FIGURE 4. Complete model TPFSDC

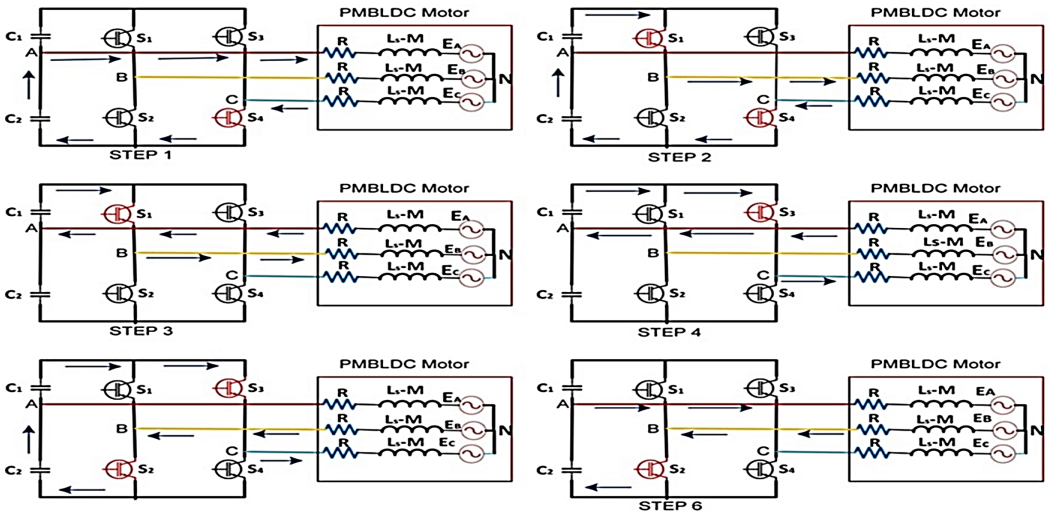

FIGURE 5. Switching patterns of TPFSDC

TABLE 2. Six-step switching sequence for TPFSDC

Steps	Switches	Active Phases	Silent Phase
1	S4	A, C	B
2	S1, S4	B, C	A
3	S1	B, A	C
4	S3	C, A	B
5	S3, S2	C, B	A
6	S2	A, B	C

CONTROL STRATEGY

Regardless of control techniques deployed in the BLDC motor, knowledge of rotor position is required in order to provide regulated voltage by the inverter to the motor. This rotor position will determine which inverter switches are active high and low. In this work, Hall-effect sensors are employed to feedback on the rotor position, which makes the commutation possible. Additionally, the PID controller is used to control the speed of the motor at the initial parameter setup from where the model simulated data was obtained for subsequent application. Consequently, the neural network from the deep learning (DL) toolbox is utilized to train and optimize this attained data by predicting the future response of the systems for enhanced performance. This control strategy is applied to both TPSSDC and TPFSDC to ascertain the best performance and control method. Table 3 shows the motor parameters used in this project.

TABLE 3. Motor Parameters

Parameters	Values	Units
Rated Voltage	500	V
Rated Speed	1000-3000	RPM
Rated Torque	5	Nm
Number of Poles	8	-
Phase Resistance	2.7850	Ohms
Phase Inductance	0.000835	H
Voltage Constant	44.8867	V.peakL-L/Krpm
Torque Constant	0.42864	Nm/A peak
Flux Linkage	0.0535795	Vs

DEEP LEARNING NEURAL NETWORK

Deep learning (DL) is a data-driving control technique. In this project, a fitting neural network from the DL toolbox was used to train and improve the system's performance. The neural network is utilized to fit data using the neural network backpropagation which trains to map between a set of input and output data. Here, the DL neural network is preferred when dealing with a signal data type where the speed measured is in time more so, it provides a flexible mechanism for solving a wide variety of tasks beyond a simple classification compared to other DL methods. In this work, data was attained by running the model at an initial PID setup where the reference input and resultant output signals were then captured and converted to data. The data was used by the fitting neural network to train and predict the feature response. After training, a neural network toolbox was generated automatically which was used in the model for optimum motor control. Figure 6 shows the DL training network.

To train the data and forecast the reaction, a DL neural network was used in order to accomplish a future response. This is done by first handling a sizable collection of data and then looking for a response within it. There are three categories for the layer. Data is received by the input layer and sent to the network for processing. The hidden layer that uses mathematical computations to forecast future responses is the next. The information obtained from the hidden layer will display an image response at the last level, the output layer.

The training state is indicated in Figure 7. The gradient at epoch 4 of 8.4315e-10 shows that learning has achieved the minimum goal. Additionally, it can be seen that as the number of epochs rises, the gradient's value decreases. The

Lavenberg-Marquardt training procedure was employed, and the network's lowest damping factor, MU 0.001, ended at 1e-05 while MU's definite value 1e-10, was used. The validation check confirms compliance with the overall network standard.

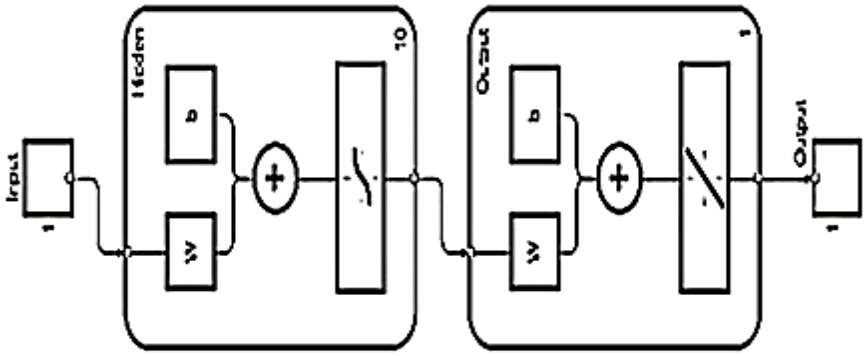

FIGURE 6. Training network

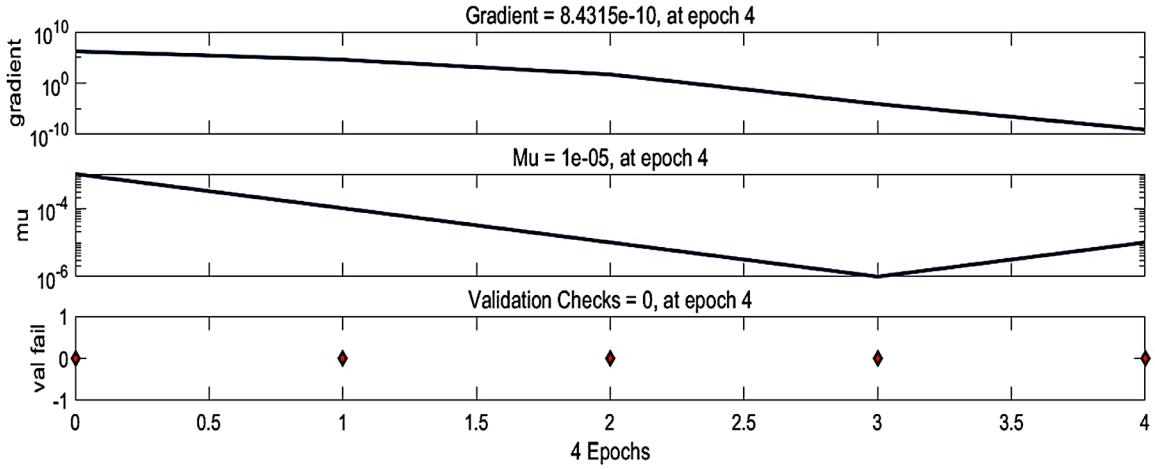

FIGURE 7. DL training state plot

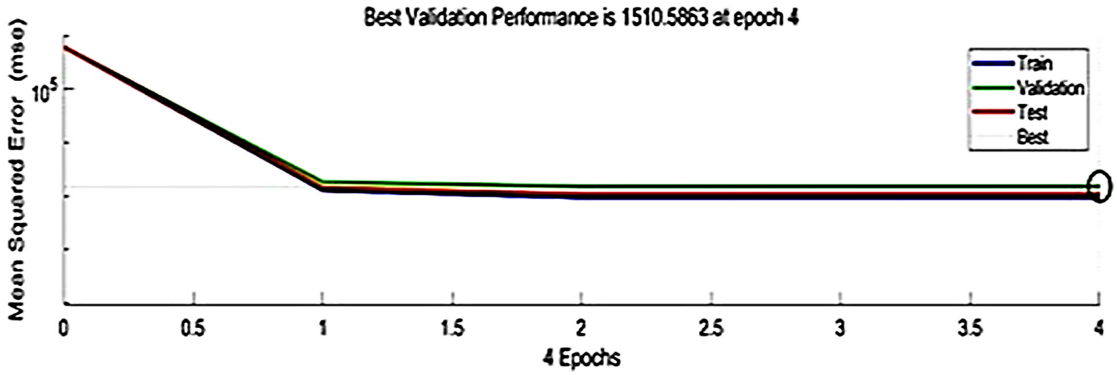

FIGURE 8. Performance plot

The performance plot in Figure 8 indicates the end of training time at epoch 4 while showing the best validation performance of 1510.5863 at epoch 4.

When looking at the histogram error plot in Figure 9, it can be observed that the instance represents the test data,

the bin displays an error of 17.12, and the training data is around 7e+04, while the validation data ranges from 7e+04 to 8.5e+04 and the test data ranges from 8.5e+04 to 10e+04. Zero error indicates the bias axis.

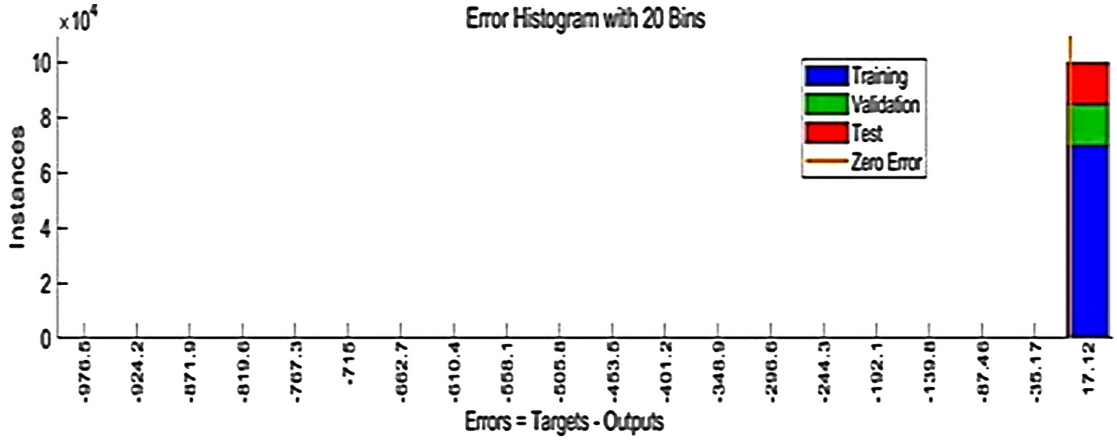

FIGURE 9. Error histogram

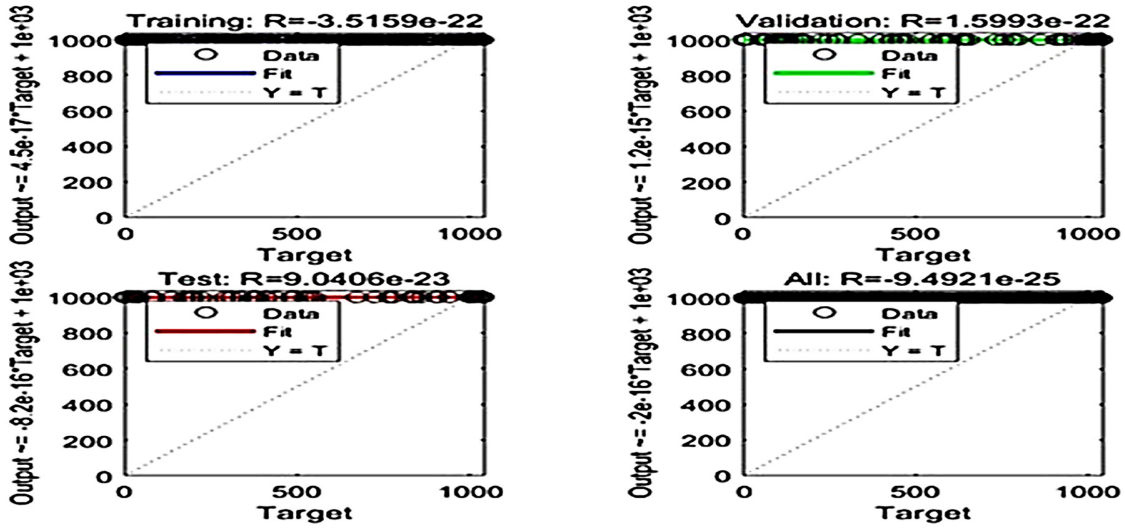

FIGURE 10. Regression plot

R in Figure 10 is the regression plot, denoting the relationship between target and output. This indicates that target and output have an exact linear relationship when R = -3.5159e-22. Based on the regression diagram above, R = 1.5993e-22 represents the data's best fit.

RESULTS AND DISCUSSION

The Simulink BLDC motor model was tested at 1000 rpm, 3000 rpm, and equally at random speeds ranging from 50 to 3000 rpm to evaluate the system's performance and flexibility during an instant speed change. The TPSSDC and TPFSDC were employed to drive and control the speed of the BLDC motor, and the resultant output was analyzed both graphically and analytically to ascertain the control strategy with the best performance considering the system overshoot, undershoot, rise time, and settling time. Also, the model's ability to reference tracks was equally accessible. The dc link voltage of 500 V was supplied to the inverter, and a 5 Nm load torque was applied as motor load. The system performance and the output results for TPSSDC and TPFSDC were compared and analyzed to attain the best results out of the two techniques.

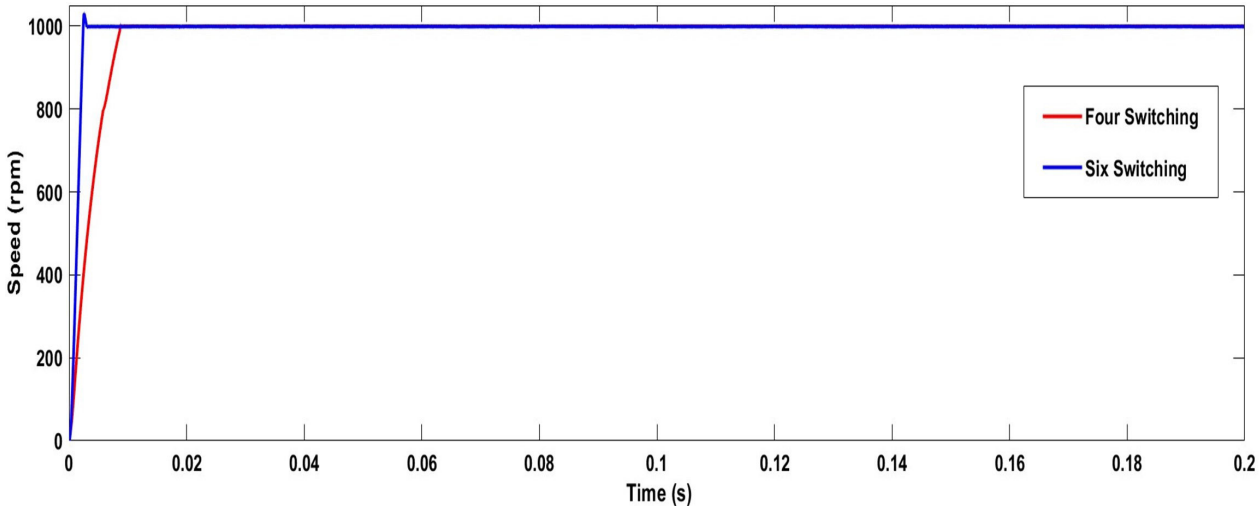

FIGURE 11. Speed responses of four- and six-switch inverters at 1000rpm

As shown in Figure 11, at 1000 rpm, both TPSSDC and TPFSDC indicate good speed tracking capability. However, it can be observed graphically that the TPSSDC outperforms the TPFSDC in terms of rise and settling times. More so, numerical values prove the same that the TPSSDC rises at 1.685 ms, which is better as compared to the TPFSDC with 6.526 ms. The settling time of 1.420 ms for TPSSDC looks equally outstanding when compared to that of TPFSDC with 5.237 ms. However, there is not much difference considering the overshoot and undershoot, as they look approximately similar.

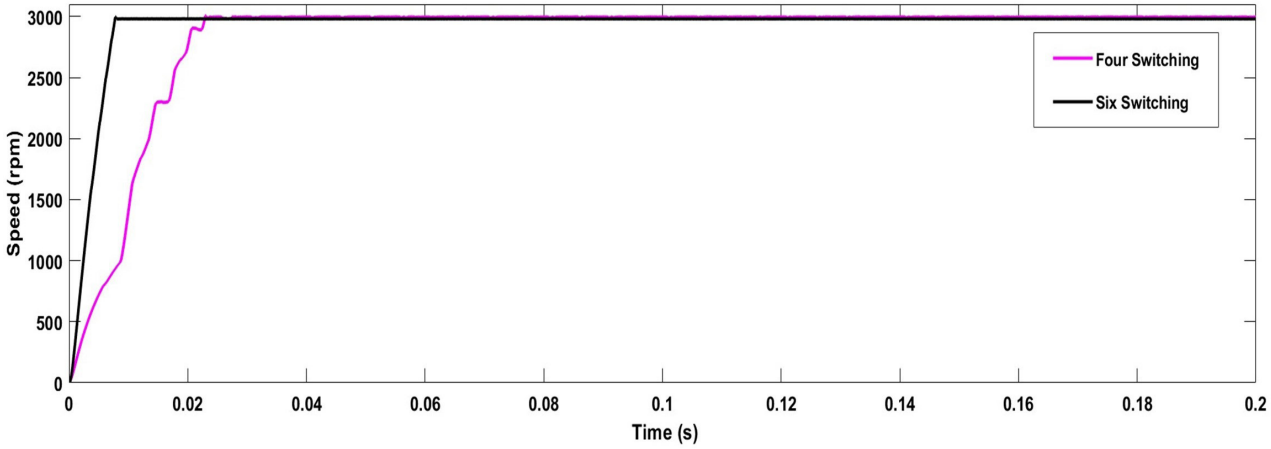

FIGURE 12. Speed response of four- and six-switch inverters at 3000rpm

Graphically, a wide difference can be observed at 3000 rpm where the TPSSDC is the favourite as it indicates good speed tracking and a better settling time than the TPFSDC, which struggles to meet the targeted speed as shown in Figure 12. Numerically, the TPSSDC rises at 5.815 ms, which beats the TPFSDC, which rises at 11.277 ms. As can also be observed, the TPSSDC settles faster at 4.048 ms as compared to the TPFSDC, which settles at 10.067 ms. Additionally, TPSSDC has a lower overshoot of 0.505% when compared to the TPFSDC's 0.685%.

At random speed, as shown in Figure 13, both the TPSSDC and TPFSDC were able to follow the reference speed, but some differences were noted during switching high or low. Even so, the TPSSDC proves better in speed tracking as it exactly meets the targeted speed at random, compared to the TPFSDC, which struggles to meet the targeted speed at 3000 rpm.

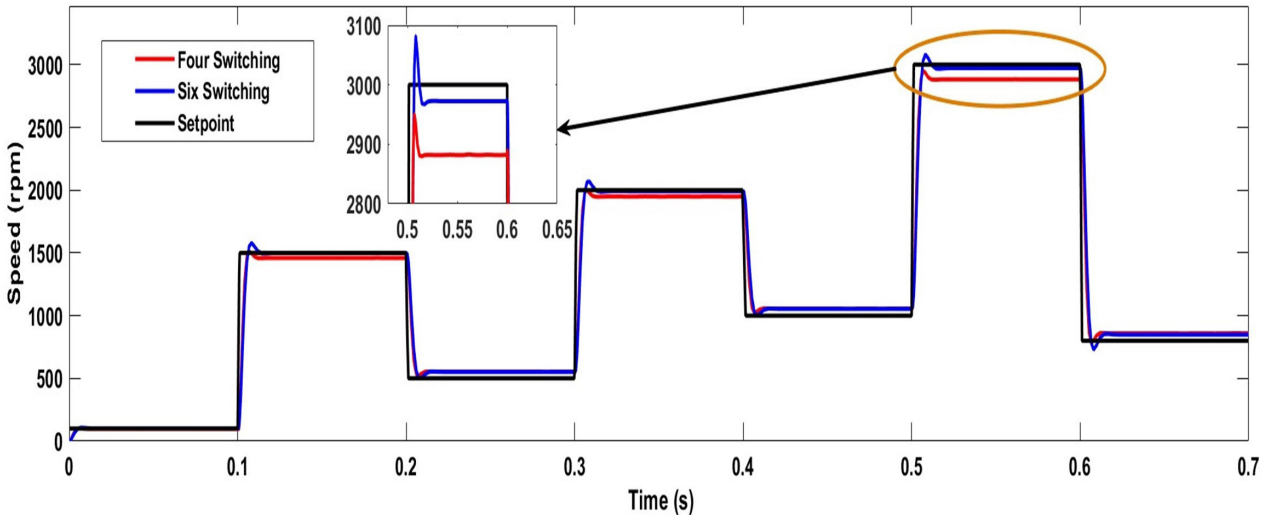

FIGURE 13. Speed response of four- and six-switch inverters at random speeds

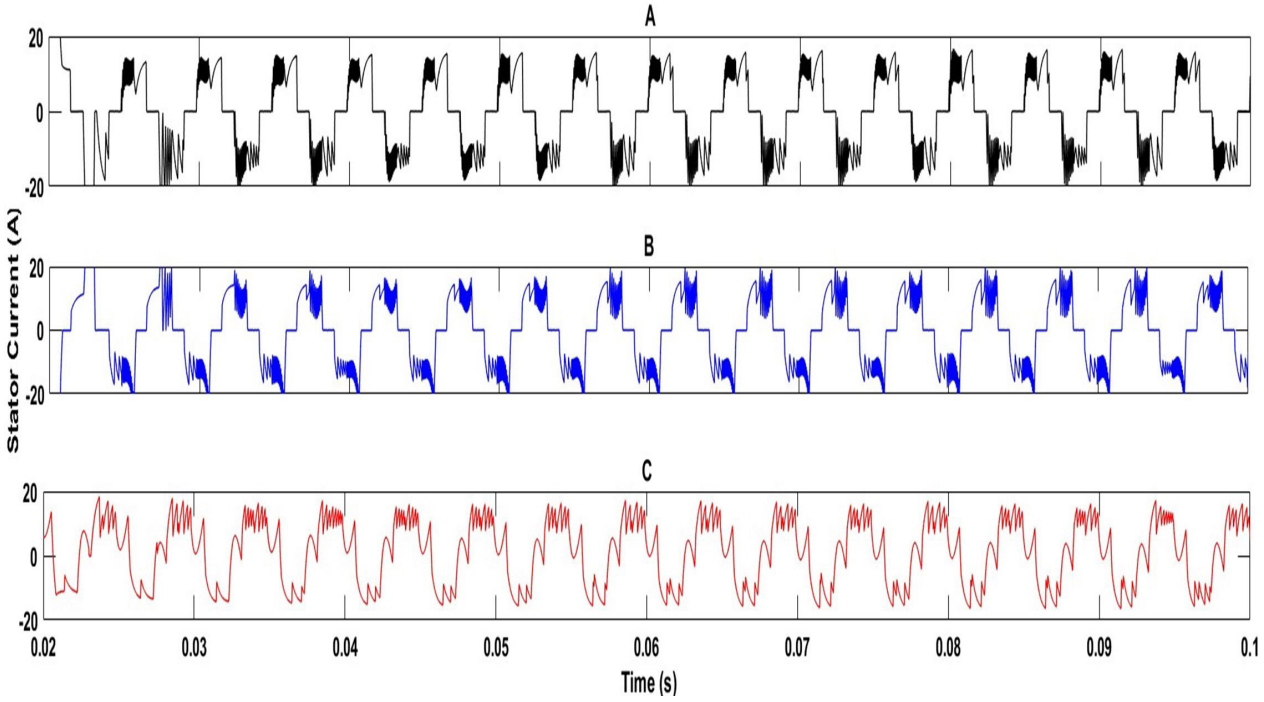

FIGURE 14. Motor phase currents in TPFSDC at 3000rpm.

Figure 14 shows the motor phase currents of TPFSDC. Some overshoot and undershoot are observed but has fewer switching ripples compared to the TPSSDC. This is a result of the smaller number of switches, which are four as compared to TPSSDC's six.

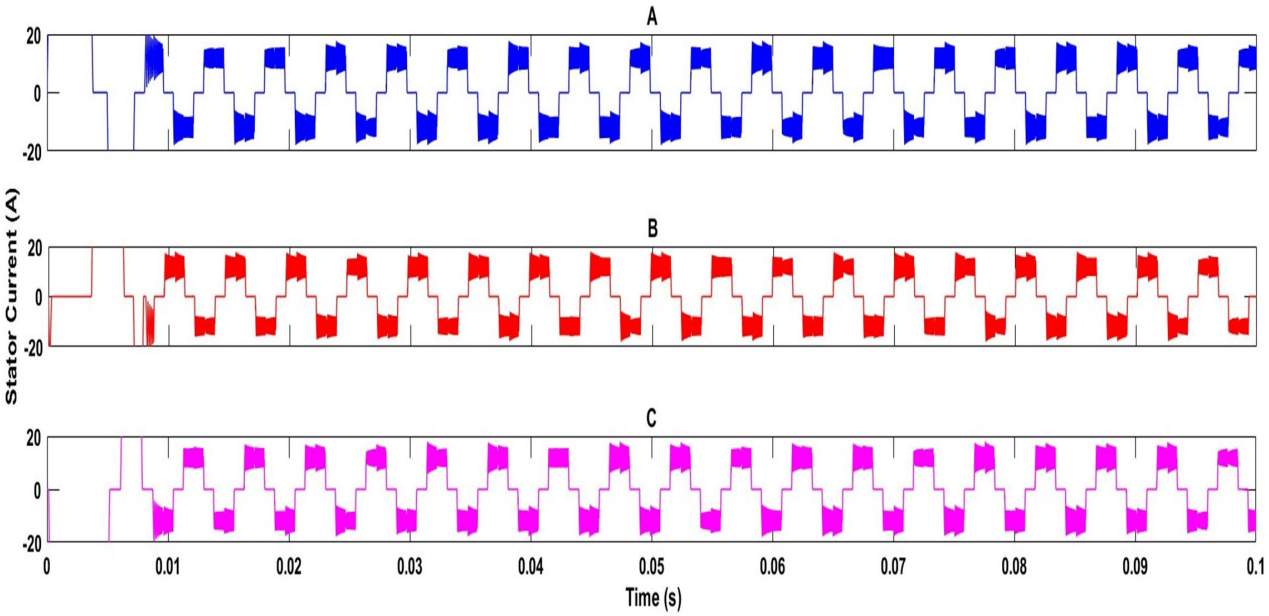

FIGURE 15. Motor phase currents in TPSSDC at 3000rpm.

The stator currents for the TPSSDC, as shown in Figure 15, look better as it is stable and have less overshoot and undershoots during switching when matched with the TPFSDC. However, high switching ripples are seen compared to the TPFSDC.

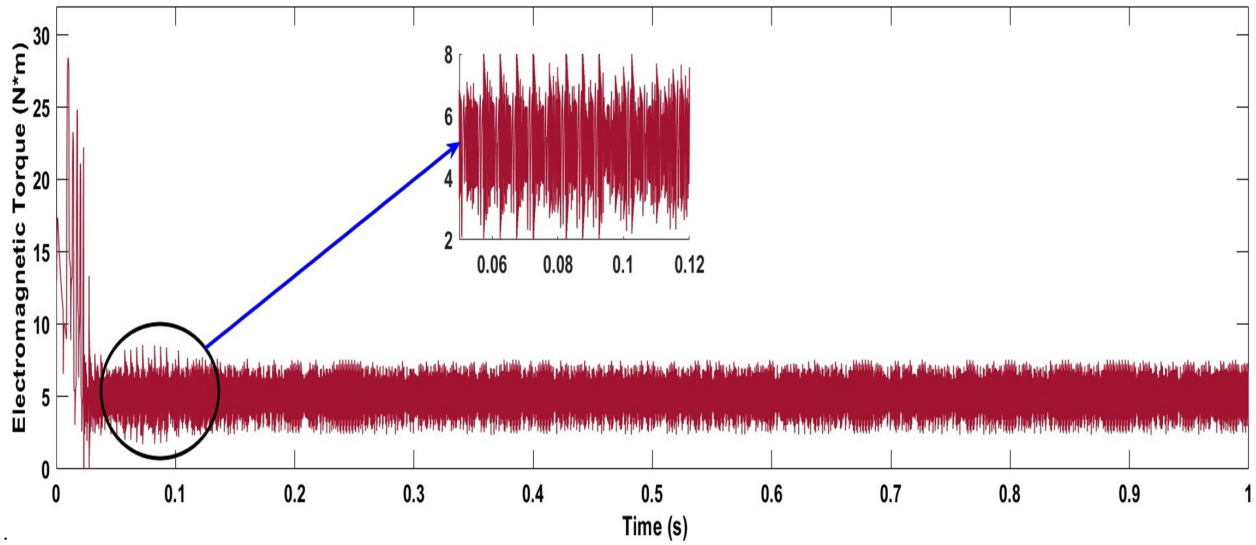

FIGURE 16. Electromagnetic torque in TPFSDC at 3000rpm

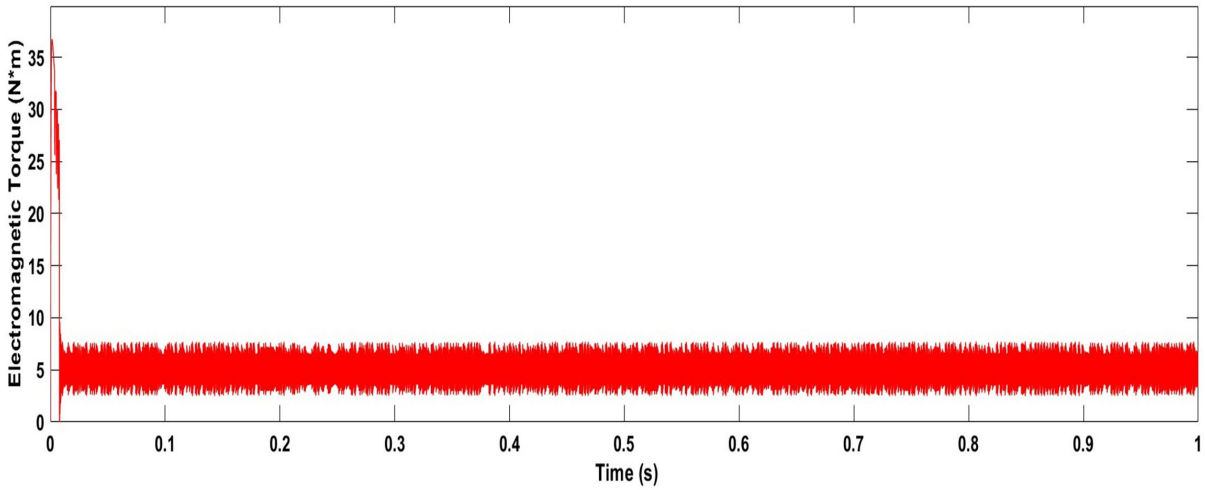

FIGURE 17. Electromagnetic torque in TPSSDC at 3000rpm

Figure 16 shows the electromagnetic torque for TPFSDC. Some instability with high ripple, and some overshoot and undershoot are also observed. This is because the capacitor terminal, which is not a switch, cannot be controlled.

Figure 17 shows the electromagnetic torque for the TPSSDC, which indicates some stability with smaller ripples and less overshoot as compared to the TPFSDC.

TABLE 4. Numerical comparisons between TPSSDC and TPFSDC

Time Responses	Four Switching		Six Switching	
	1000rpm	3000rpm	1000rpm	3000rpm
Rise Time	6.526ms	11.277ms	1.685ms	5.815ms
Settling Time	5.237ms	10.067ms	1.420ms	4.048ms
Overshoot i	0.505%	0.685%	0.521%	0.505%
Undershot	2.000%	2.000%	1.997%	1.999%

Thus, numerical values in Table 4 precisely validate the graphical results. Hence, it is clear that the TPSSDC is better when compared with the TPFSDC employing the DL control strategy.

CONCLUSION

Based on this research work, it can be concluded that the neural network control approach was able to minimize the system overshoot and undershoot as well as improve the system rise and settling time in both the four and six driving topologies. However, it was seen that the TPSSDC proves to be a better option for driving a three-phase, permanent magnet BLDC motor. Graphical observation also confirms the TPSSDC is the preferred technique for its good reference tracking, minimum ripple, and better rise and settling times when matched with the TPFSDC method. Numerical values also validate the graphical results, as it can be seen that at 1000 rpm, the TPSSDC rises at 1.685 ms and settles at 1.420 ms, while the TPFSDC rises at 6.526 ms and settles at 5.237 ms. Also, at 3000 rpm, the TPSSDC rises at 5.815 ms and settles at 4.048 ms, compared to the TPFSDC, which rises at 11.277 ms and settles at 10.067 ms. Hence, the TPSSDC outperforms the TPFSDC. However, the TPFSDC is preferred economically because there are fewer switches and the topological arrangement is less complex.

ACKNOWLEDGEMENT

The authors would like to thank the Petroleum Technology Development Fund (PTDF) of Nigeria for providing the sponsorship and financial support for this research.

DECLARATION OF COMPETING INTEREST

None

REFERENCES

Al Mashhadany, Y. I. M., Abbas, A. K., & Algburi, S. S. 2022. Modeling and analysis of brushless DC motor system based on intelligent controllers. *Bulletin of Electrical Engineering and Informatics* 11(6): 2995–3003. https://doi.org/10.11591/eei.v11i6.4365

Ale, B. 2022. Modeling and Performance Analysis of an In-wheel Permanent Magnet Brushless DC (PM BLDC) Motor in MATLAB. *Applications of Modelling and Simulation* 6: 150–157. http://arqiipubl.com/ams

Archana Mamadapur, & Dr.Unde Mahadev G. 2019. Speed Control of BLDC Motor Using Neural Network Controller and PID Controller. Proceedings of the 2019 2nd International Conference on Power and Embedded Drive Control (ICPEDC) : 21-23 August 2019, SSN College of Engineering, Kalavakkam, Chennai, India., 146–151. https://doi.org/10.1109/ICPEDC47771.2019.9036695

Arun Prasad, K. M., & Nair, U. 2020. Intelligent fuzzy sliding mode controller based on FPGA for the speed control of a BLDC motor. *International Journal of Power Electronics and Drive Systems* 11(1): 477–486. https://doi.org/10.11591/ijpeds.v11.i1.pp477-486

de Almeida, P. M., Valle, R. L., Barbosa, P. G., Montagner, V. F., Cuk, V., & Ribeiro, P. F. 2020. Robust control of a variable-speed BLDC motor drive. *IEEE Journal of Emerging and Selected Topics in Industrial Electronics* 2(1): 32–41. https://doi.org/10.1109/jestie.2020.3035055

Didi Susilo Budi Utomo. 2017. Model Reference Neural Adaptive Control Based BLDC Motor Speed Control. 2017 5th International Conference on Electrical, Electronics and Information Engineering (ICEEIE), 49–54. https://doi.org/10.1109/ICEEIE.2017.8328761

Gujja, M. M., & Ishak, D. 2023. Comparative Evaluation and Analysis of Six- and Four-Switch Drivers for PMBLDC Motor Control. 2023 International Conference on Energy, Power, Environment, Control, and Computing (ICEPECC), 1–6. https://doi.org/10.1109/ICEPECC57281.2023.10209482

Huang, C. L., Wu, C. J., & Yang, S. C. 2020. Model reference adaptive control of pulse amplitude modulated pm motor drive for high power transport drone applications. ECCE 2020 - IEEE Energy Conversion Congress and Exposition, 2977–2981. https://doi.org/10.1109/ECCE44975.2020.9236063

L. Saleh, A., A. Obed, A., H. Qasim, H., I.H. Breesam, W., I.A. Al-Yasir, Y., Ojaroudi Parchin, N., & A. Abd-Alhameed, R. 2021. Wavelet neural networks for speed control of BLDC motor. In Automation and Control (pp. 1–21). IntechOpen. https://doi.org/10.5772/intechopen.91653

Lajić, R., & Matić, P. 2022. Speed control of bldc motor with ripple effect reduction using recurrent wavelet neural networks. *IJEEC - International Journal of Electrical Engineering and Computing* 6(2): 57–64. https://doi.org/10.7251/ijeec22020571

Mohd Zaihidee, F., Mubin, M., Seng Che, H., & Jing Rui, T. 2022. Development of closed-loop permanent magnet synchronous motor drive system prototype. *Jurnal Kejuruteraan* si5(2), 79–90. https://doi.org/10.17576/jkukm-2022-si5(2)-09

Naseri, F., Farjah, E., Schaltz, E., Lu, K., & Tashakor, N. 2021. Predictive control of low-cost three-phase four-switch inverter-fed drives for brushless DC motor applications. *IEEE Transactions on Circuits and Systems I: Regular Papers* 68(3): 1308–1318. https://doi.org/10.1109/TCSI.2020.3043468

Özge Gülbaş, Yakup Hameş, & Murat Furat. 2020. Comparison of PI and Super-twisting Controller Optimized with SCA and PSO for Speed Control of BLDC Motor. 2020 International Congress on Human-Computer Interaction, Optimization and Robotic Applications (HORA), 1–7. https://doi.org/10.1109/HORA49412.2020.9152853

Pamuji, F. A., Prihantari, kharisma J., Riawan, D. C., Asfani, D. A., Suryoatmojo, H., Guntur, H. L., Sudarmanta, B., & Arumsari, N. 2022. Application of artificial neural network for speed control of BLDC motor 90KW in electrical bus. *Przeglad Elektrotechniczny* 98(2): 203–210. https://doi.org/10.15199/48.2022.02.47

Reddy, Ch. L., Kumar, P. S., Rao, J. V. G. R., & Sharanya, M. 2023. Performance analysis of switched reluctance motor by using closed loop current control technique. *Jurnal Kejuruteraan* 35(6): 1393–1401. https://doi.org/10.17576/jkukm-2023-35(6)-12

Safak Ekemen, Bekir Fincan, & Murat Imeryuz. 2016. A BLDC Motor Drive with Four Switch Three Phase Inverter. 2016 IEEE International Conference on Renewable Energy Research and Applications (ICRERA), 804–808. https://doi.org/10.1109/ICRERA.2016.7884447

Saleh, I., Bature, A. A., Buyamin, S., & Shamsudin, M. A. 2022. Speed control of a BLDC motor using artificial neural network with ESP32 microcontroller based implementation. Sringer Lecture Notes in Electrical Engineering, 921 LNEE, 358–368. https://doi.org/10.1007/978-981-19-3923-5_31

Surabhi Agrawal, & Vivek Shrivastava. 2017. Particle swarm optimization of BLDC motor with fuzzy logic controller for speed improvement. 2017 8th International Conference on Computing, Communication and Networking Technologies (ICCCNT), 1–5. https://doi.org/10.1109/ICCCNT.2017.8204006

Vanchinathan, K., Valluvan, K. R., Gnanavel, C., & Gokul, C. 2021. Design methodology and experimental verification of intelligent speed controllers for sensorless permanent magnet Brushless DC motor. *International Transactions on Electrical Energy Systems* 31(9). https://doi.org/10.1002/2050-7038.12991

Vikhe, P. S., Shukla, B. S., Kadu, C. B., & Mandhare, V. V. 2019. Speed control of BLDC motor using open loop, PID controller and neural network. *International Journal of Engineering and Advanced Technology* 9(1): 2210–2213. https://doi.org/10.35940/ijeat.A9710.109119

Wang, T., Wang, H., Hu, H., & Wang, C. 2020. LQR optimized BP neural network PI controller for speed control of brushless DC motor. *Advances in Mechanical Engineering* 12(10). https://doi.org/10.1177/1687814020968980

Yao, G., Feng, J., Wang, G., & Han, S. 2023. BLDC motors sensorless control based on MLP topology neural network. *Energies* 16(10). https://doi.org/10.3390/en16104027